

Enhancing the Optoelectronic Properties of Solution-Processed AgInSe₂ Thin Films for Application in Photovoltaics

Shubhanshu Agarwal, Kyle Weidemann, David Rokke, Kiruba Catherine Vincent, and Rakesh Agrawal*

Davidson School of Chemical Engineering, Purdue University, West Lafayette, Indiana 47907, United States

*Email: agrawalr@purdue.edu

Abstract

AgInSe₂ is a promising direct bandgap thin-film material with a rare n-type conductivity. Similar to thin film photovoltaic materials such as Cu(In,Ga)Se₂ (CIGSe), which have achieved efficiencies as high as ~23%, AgInSe₂ also crystallizes in a chalcopyrite phase while also being more tolerant to antisite defects due to higher defect formation energies resulting from more significant variations in cation sizes. AgInSe₂ has a suitable bandgap of 1.24 eV, which lies in the high-efficiency region of the detailed balance limit. In this work, we have utilized a Dimethyl Formamide-Thiourea-Chloride-based solution-processed route to deposit a thin film of AgInS₂ which is converted into AgInSe₂ after a heat-treatment step in a selenium environment. AgInSe₂ optoelectronic properties depend on the Ag/In ratio and the selenium heat-treatment conditions. Significant improvements in photoluminescence yield and lifetime are observed for Ag-poor films in selenium-rich conditions. X-ray Photoelectron Spectroscopy (XPS) measurements confirm a higher amount of selenium on the surface of films with improved optoelectronic properties. Furthermore, a high minority carrier lifetime of 9.2 ns and a Photoluminescence Quantum Yield (PLQY) of 0.013% is obtained without any passivating layer, which improved to 0.03% after CdS passivation. Hall effect measurements confirm that AgInSe₂ has n-type conductivity with a moderate carrier concentration (10^{14} cm^{-3}), more suitable for a p-i-n architecture. XPS has further confirmed the moderate n-type conductivity.

Introduction

For the worldwide use of solar energy to lead to a green energy economy, we need photovoltaic materials that are low-cost, stable, have good optoelectronic and charge transport properties, and can be easily manufactured on a large scale. Thin-film solar cells show all these characteristics, some of which have surpassed the monocrystalline Si efficiency.¹ Among thin-film devices, CdTe and CuInSe₂/Cu(In,Ga)Se₂ (CIS/CIGSe) are among the most promising. CIGSe has achieved a lab-record efficiency of 23.35% and can be produced by solution processing techniques.²⁻⁴ However, the propensity of copper cations to exist in two oxidation states results in lower formation energy for copper-based defects in the CIGSe crystal lattice.⁵⁻⁷ Replacing

copper with silver in ClSe may be helpful as Ag only has a +1 oxidation state and has a larger cation size than In^{+3} and Ga^{+3} , significantly increasing the defect formation energy.^{8,9} ClSe , however, has a bandgap of 1.0 eV, which is not suited for single-junction PV applications, whereas AgInSe_2 has a larger bandgap of 1.24 eV, closer to the ideal 1.4 eV bandgap predicted by the detailed balance limit.¹⁰⁻¹² AgInSe_2 is also thermodynamically stable and has good electronic properties.¹³⁻¹⁵ It is n-type, which is different from ClSe/CIGSe , but the structural similarities with CIGSe could be a good sign for the viability of this material. All these favorable properties of silver addition have warranted a need to study AgInSe_2 in detail. However, there is only one instance in literature where a solar device has been fabricated from AgInSe_2 . Agel et al. grew an n-type AgInSe_2 film on a p-type Si substrate.¹⁶ They achieved a conversion efficiency of 2.71%, and the device showed Schottky diode-like characteristics. These numbers look promising for a material that has been scarcely studied and optimized.

In most cases, AgInSe_2 films have been prepared using costly vacuum processing techniques.^{11,14-21} These techniques require a high vacuum, have inefficient material utilization, and involve batch processing.^{22,23} Solution processing is a cost-effective alternative for rapidly commercializing promising materials such as AgInSe_2 . It works at ambient pressure conditions, has a more efficient material utilization, and can be used in the roll-to-roll manufacturing of thin-film absorber films.²⁴ However, in the literature, there are no reports of a solution-processed AgInSe_2 film other than a recent Ph.D. thesis.²⁵ Hence, our research goal is to fabricate a solution-processed AgInSe_2 film with good optoelectronic properties for incorporation into a solar cell.

Limited research has been done on AgInSe_2 despite its promising properties. Hence, this work aims to fabricate and characterize solution-processed AgInSe_2 films for their potential use in solar cells. We have utilized the benign N-N Dimethyl Formamide (DMF)-Thiourea (TU)-Chlorides chemistry to cast AgInS_2 thin film, which is further heat-treated in a selenium environment to form AgInSe_2 film. We have optimized the composition and selenization conditions to lower the defects in AgInSe_2 films and achieved high Photoluminescence Quantum Yield (PLQY). We have further done advanced characterizations to evaluate the electrical properties and the band positions.

Experimental

Materials Silver (I) Chloride (99.999%), Indium (III) Chloride (99.999%), Thiourea (99.98%), N-N Dimethylformamide (>99.8%), Butylamine (>99.5%), 1,2-Ethanedithiol (>99%), alumina dispersed in 2-propanol (20 wt%), and SeCl_4 were obtained from Sigma Aldrich. Selenium used in selenization (5mm pellets, 99.999%) and Selenium powder (99.99%) were obtained from Millipore Sigma. All chemicals were used as received except for the Thiourea, which was twice recrystallized from 18.2 $\text{M}\Omega$ Deionized Water and dried under vacuum, followed by an ambient-pressure drying in the air overnight at 90°C. Corning's alkali-free Eagle XG (EXG) glass substrates were obtained from Stemmerich. All chemicals were stored in nitrogen-filled glove boxes.

Ink Preparation Ink preparation was performed in a nitrogen-filled glove box. DMF-TU-Chlorides chemistry was utilized to prepare the molecular precursor ink, which uses AgCl and InCl_3 as the Ag and In metal precursors. Since AgCl is photosensitive, it was always handled in the dark. In most experiments, 0.8 M total metal concentration was maintained in ink, and the Ag/In ratio

was varied. Moreover, 1.6 M TU concentration was maintained in DMF, and AgCl and InCl₃ were sequentially added to the TU+DMF solution to prepare the ink. The ink was then vortexed and stirred on a heated stir plate at 35 °C. Before coating, the ink was filtered with a 0.45-micron pore-sized PTFE membrane syringe filter.

A 1.2 M total metal concentration ink was also used with a 3.8 M TU concentration to achieve a relatively thick film.

Molybdenum and Alumina Deposition Before molybdenum or alumina deposition, EXG glass was thoroughly rinsed with DI water, 2-propanol, and methanol and then sonicated in an Alconox bath followed by sonication in DI water. The glass was then cleaned in a UV-ozone cleaner for 30 min.

The glass was loaded in a PVD chamber for molybdenum deposition and 800 nm thick molybdenum layer was sputtered at an ultralow vacuum.

For film growth on alumina-coated glass, the commercial alumina nanoparticles solution was initially diluted by combining 0.2 ml of commercial alumina solution with 1.8 ml 2-propanol. The solution was then spin-coated on the cleaned EXG glass at 1000 RPM for 1 min, followed by 1 min annealing at 100 °C and 30 min annealing at 500 °C.

Film Coating The DMF-Thiourea-Chlorides ink was coated on a molybdenum or alumina-coated EXG glass substrate (which contains no sodium) to fabricate AgInS₂ thin films. Unless specified, the film is coated on molybdenum in this report. The coating procedure was performed on an automated spin coater in a nitrogen-filled glove box. 200 μ l of ink was used in each cycle with the substrate holder rotating at 3000 RPM for 30 seconds, followed by a 30-second wait time for the ink to dry. The sample was then transferred to a hot plate set at 300 °C, and the film was annealed for 90 seconds. The film was then cooled on an aluminum block. This coating cycle was repeated 14 times with 0.8 M total metal concentration ink to achieve a film of the desired thickness. 10 coating cycles were used instead with an ink of 1.2 M total metal concentration to achieve thicker films.

Regular Selenization The next step involved annealing the sulfide AgInS₂ film in a selenium environment in a refractory tube furnace following the procedure for selenization of Cu(In,Ga)S₂ films.²⁶ In a regular selenization setup, the sample rested on the floor of a graphite box with selenium pellets arranged around it, as shown in **Figure 1a**. Before ramping up the temperature, the tube furnace was purged using a vacuum and argon purge cycle multiple times to remove the oxygen. Then, the furnace temperature was ramped up to the desired setpoint (475-600 °C), and the film was annealed in a selenium environment for 20 minutes.

Modified Selenization with glass shims A modified selenization setup was used to increase the selenium supply to the film during the heat-up period. In this setup, the sample rested on two small pieces of EXG glass near the far edges of the 1" x 0.5" film, shown in **Figure 1b**. This arrangement avoided any direct contact of the sample with the graphite box, which has high absorptivity and thermal conductivity and thus quickly heats the sample if it rests directly on the graphite surface. However, the selenium pellets were still in contact with the graphite floor and volatilized normally, the volatility rate set by the graphite floor temperature. The sulfide film

heated up slowly because of increased thermal resistance from the glass shims, resulting in a significant difference in temperature between the selenium vapors and the film's surface, causing higher selenium condensation onto the film. Hence, this modified setup had more liquid Se on the film. Simplified numerical heat transfer calculations in **Figures S1 and S2** and Weidemann's doctoral thesis support the above discussion.²⁷

Other Selenization Methods Other selenization methods with higher selenium availability were also employed. In the first case, an additional 0.4 M selenium ink in Butylamine + 1,2-Ethanedithiol was prepared, and two layers of this ink were coated on top of the AgInS₂ film. The film was then annealed at 100 °C for two minutes to remove the solvents. This provided a thick layer of Se on the AgInS₂ film that could act as a selenium source during selenization. This modified film was further selenized by regular selenization (no shims used). In another method, 25 mg selenium powder was spread on the AgInS₂ film, which also acted as the selenium source during selenization. This film was also selenized via regular selenization.

Characterization Raman spectroscopy was performed using a Horiba/Jobin-Yvon HR800 Raman spectrometer with a 632.8 nm excitation laser wavelength. A quartz cuvette enclosed in a nitrogen atmosphere was used for collecting spectra on liquid solutions. X-ray diffraction was performed in a Rigaku SmartLab Diffractometer under ambient conditions in parallel beam geometry with an incident beam angle of 0.5 degrees using a Cu K α source ($\lambda = 1.5406 \text{ \AA}$) operating at 40kV and 44mA. Hall effect measurements were performed on a LakeShore M91 FastHall with magnetic field strengths from -9 Tesla to 9 Tesla.

Time-resolved photoluminescence (TRPL) was acquired by the single photon counting technique using a 640 nm diode laser (pulse width of 100 ps, 1 MHz) and an InGaAs photomultiplier tube (Hamamatsu H10330-75).

The obtained TRPL decay curves were fitted with biexponential fits, and the statistical average of the lifetime values was reported. The statistical average is given by:

$$\tau_{stat} = \frac{B_1\tau_1 + B_2\tau_2}{B_1 + B_2}$$

B_1 and B_2 are the pre-exponential factors, and τ_1 and τ_2 are the characteristic minority carrier lifetimes.

Photoluminescence measurements were performed with a Horiba LabRAM HR800 using a 632.8nm He:Ne laser and a liquid nitrogen-cooled InGaAs detector. Spectral corrections were performed by comparing the normalized measured spectrum of a calibrated light source (Avantes Avalight HAL-CAL MINI) with the known normalized spectrum provided by the vendor, as detailed in a previous report.²⁸ Further apparatus calibration was performed to obtain quantitative photoluminescence, as detailed in Rokke's doctoral thesis.²⁵

The XPS data was obtained at the Surface Analysis Facility of the Birck Nanotechnology Center, Purdue University. X-ray photoelectron spectroscopy (XPS) measurements were performed using

a Kratos Axis Ultra DLD imaging XPS instrument with a monochromatic Al K α (1486.6 eV) radiation and a chamber pressure of less than 2E-09 Torr. The samples were transferred immediately to a argon-filled glovebox after selenization to avoid oxygen contamination and were then vacuum sealed to transfer to the XPS instrument. The vacuum seal was broken inside a glovebox connected to the XPS instrument. For the XPS data analysis CASAXPS software was used. The spectra were charge-corrected using the C1s peak. The data was charge corrected using the C1s peak set at 284.8 eV.

Scanning electron microscopy (SEM) measurements were performed on the FEI Quanta three-dimensional system with an Everhart-Thornley detector at an accelerating voltage of 7 kV with a working distance of 10 mm.

Fisher XAN 250 X-ray fluorescence (XRF) instrument at 50 kV voltage with a primary Ni filter containing a silicon drift detector was used to measure the bulk composition. We have reported XRF-measured composition rather than the nominal composition in this work.

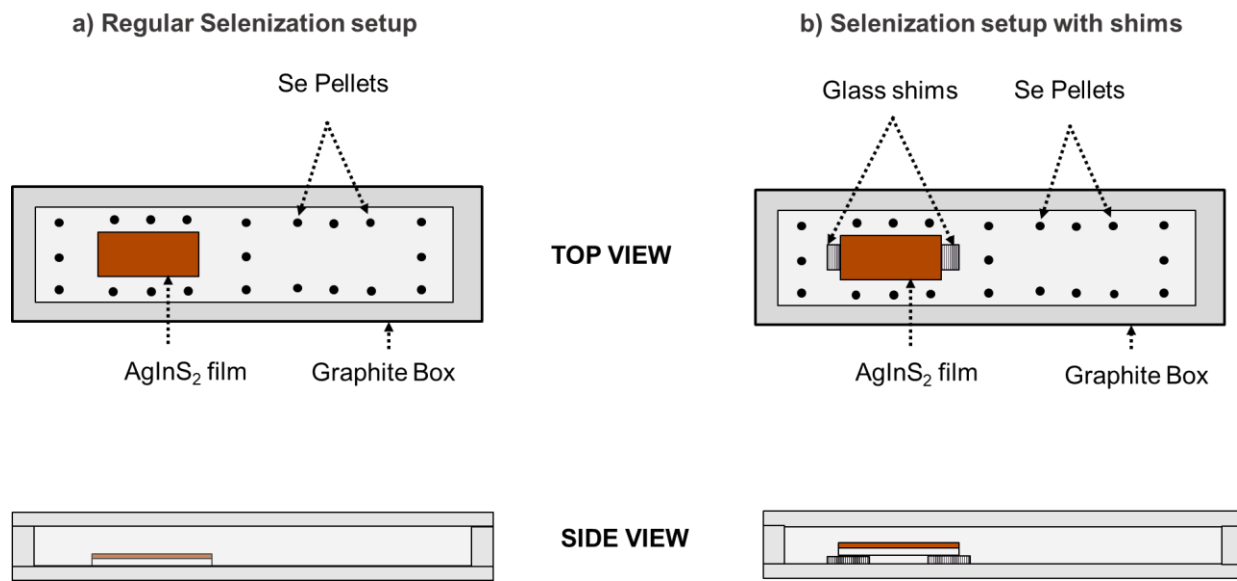


Figure 1. Schematic showing the difference between the (a) regular selenization setup and the (b) selenization setup with shims.

Results and Discussions

Solution-Processed AgInSe₂

In the only reported case of solution-processed AgInSe₂ film, Ag₂S and In as the metal precursors were dissolved in Butylamine and 1,2-Ethanedithiol to prepare a stable ink.²⁵ However, this approach had some challenges: a) the films had a poor PL yield, b) their minority carrier lifetime was low at around 300 ps, and c) the amines and thiols are toxic.

All the above challenges motivated us to search for other benign chemistries. We explored the DMF-Thiourea-Chlorides route, which is reported to produce carbon-free CuInSe_2 thin films.⁷ DMF, a Lewis basic aprotic solvent, cannot solvate monovalent cations, such as Ag^+ , on its own. However, adding TU stabilizes the Ag^+ cation, and the solubility of AgCl increases when at least two mol of TU are present per mol of AgCl . The 0.4 M AgCl with 0.4 M TU in DMF did not dissolve. However, 0.4 M AgCl dissolved completely with 0.8 M and higher TU concentrations in DMF. Liquid Raman measurements verify an interaction of AgCl and TU owing to the gradual peak broadening and peak shift of the 744 cm^{-1} C=S stretch, as shown in **Figure 2**. Thiourea also increases the solubility of InCl_3 by reacting with the free Cl^- in the solution and increasing the concentration of highly soluble $[\text{InCl}]^{2+}$ species.⁷ **Figure 3** shows the as-coated AgInS_2 films from the equimolar AgCl and InCl_3 ink which form densely packed flower-shaped grains via this route showed the orthorhombic phase as opposed to the chalcopyrite phase observed in the literature at these temperatures. Surprisingly, the as-coated film showed an intense PL emission with a broad spectrum centered at 1.18 eV, possibly originating from a midgap defect in AgInS_2 or some secondary phases, as evidenced by **Figure S3**. More work is needed to assign this PL peak correctly. **Figure 4c** indicates the as-coated stoichiometric orthorhombic AgInS_2 film converted to chalcopyrite AgInSe_2 film after selenization. We potentially accessed an Ag_2Se liquid flux that helped nucleate and grow large AgInSe_2 grains similar to those reported for other material systems.²⁹⁻³¹ The selenized film has irregularly shaped grains when selenized with regular selenization conditions, as shown in **Figures 4a** and **4b**. **Figure S4** shows the film also has residual carbon. The photoluminescence for the film is centered at 1.25 eV with a narrow FWHM of 59 meV, but the intensity was relatively low. The PLQY yield and the minority carrier lifetimes were poor for the stoichiometric film under all conditions of regular selenization with PLQY less than 1E-04% and a lifetime less than 300 ps, shown in **Figures 4d** and **4e**. We tried selenizations at temperatures between 475 and 525 °C but saw no improvements. These results suggest the presence of intrinsic defects in the AgInSe_2 fabricated under these conditions.

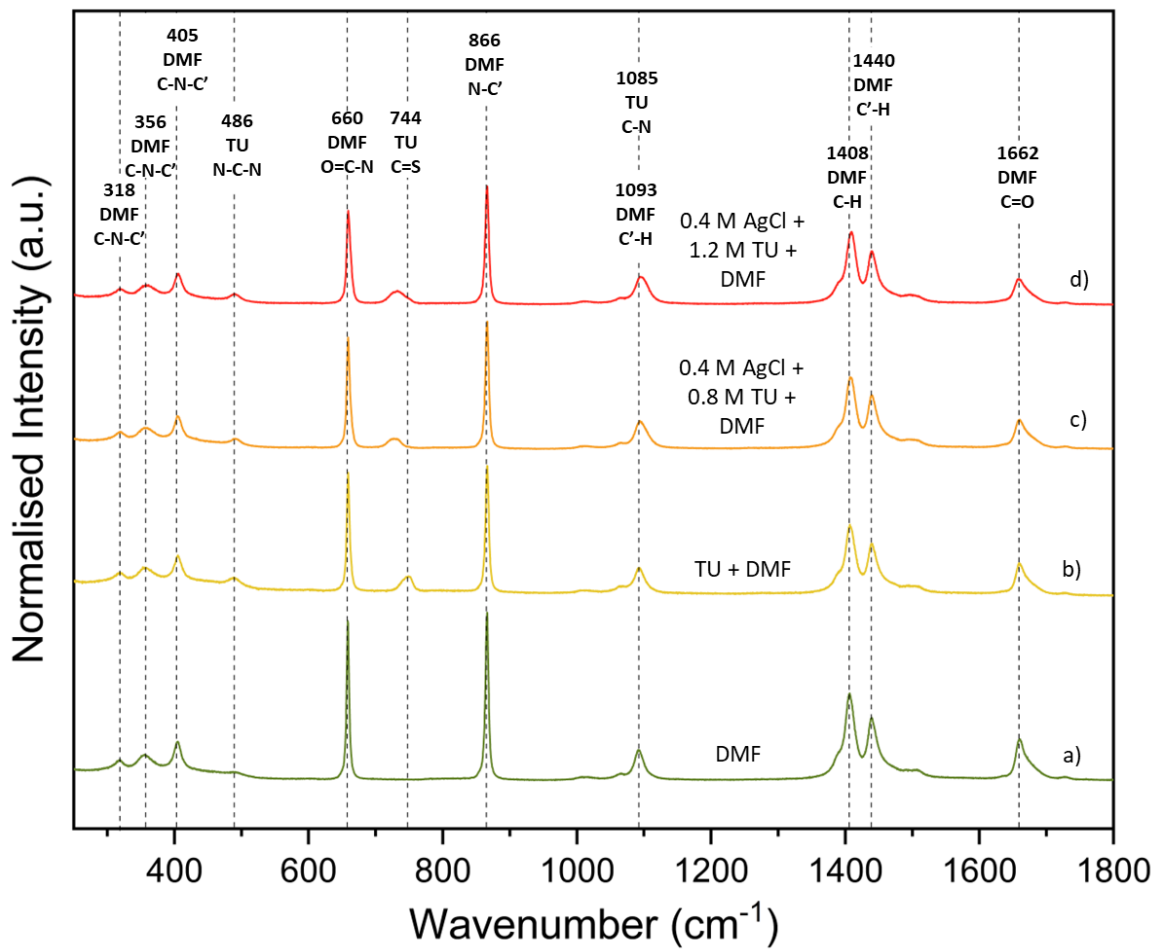


Figure 2. Liquid Raman on a) only Dimethyl Formamide (DMF), b) Thiourea (TU) + DMF, c) AgCl (0.4 M) + TU (0.8 M) + DMF, d) AgCl (0.4 M) + TU (1.2 M) + DMF. The peak shift in the C=S bond stretch of TU suggests a metal-sulfur interaction.

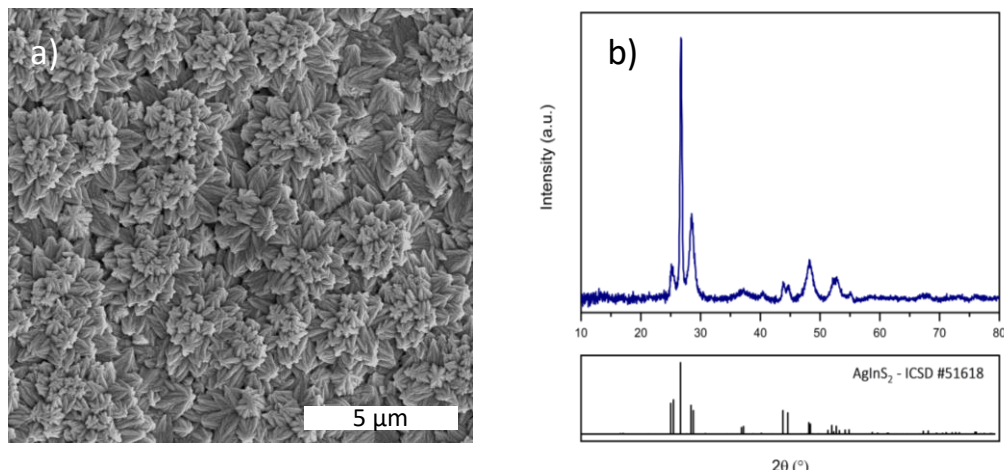


Figure 3. a) SEM image, b) XRD pattern of as-coated AgInS₂ film annealed at 300 $^{\circ}\text{C}$.

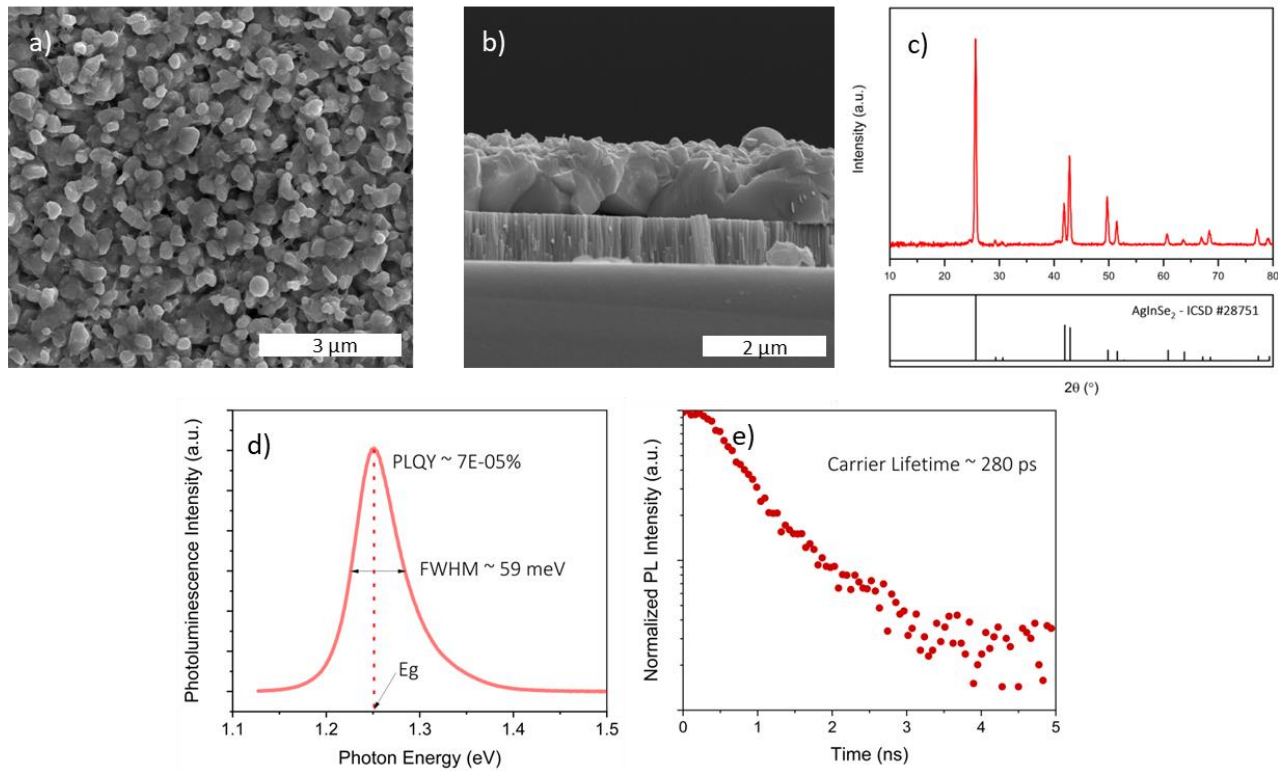


Figure 4. a) SEM top-view, b) SEM cross-sectional view, c) XRD pattern, d) Photoluminescence plot, and e) TRPL decay curve of stoichiometric AgInSe_2 film selenized at 500 $^{\circ}\text{C}$ with regular selenization (arrangement of Figure 1a).

Effect of Ag/In ratio on the Optoelectronic Properties of AgInSe_2

We also varied the Ag/In ratio in the solution-processed AgInSe_2 films produced via the DMF-Thiourea-Chlorides chemistry to study its impact on optoelectronic properties. For $\text{Ag/In} < 1$ (Ag-poor), we observed slight improvements in PL and lifetime similar to CISe/CIGSe . These improvements continued for Ag/In as low as 0.9, where they started forming a secondary phase of AgIn_5Se_8 , as shown in **Figure 5a**. Although there was an improvement in PL and carrier lifetime, the numbers were still relatively low, as shown in **Figure 5b**. These improvements were possibly due to the formation of benign defect complexes for Ag-poor films, such as $2\text{V}_{\text{Ag}} + \text{In}_{\text{Ag}}$, similar to those reported for CuInSe_2 .³² While Ag-poor AgInSe_2 composition seems favorable, other defects may also limit the performance.

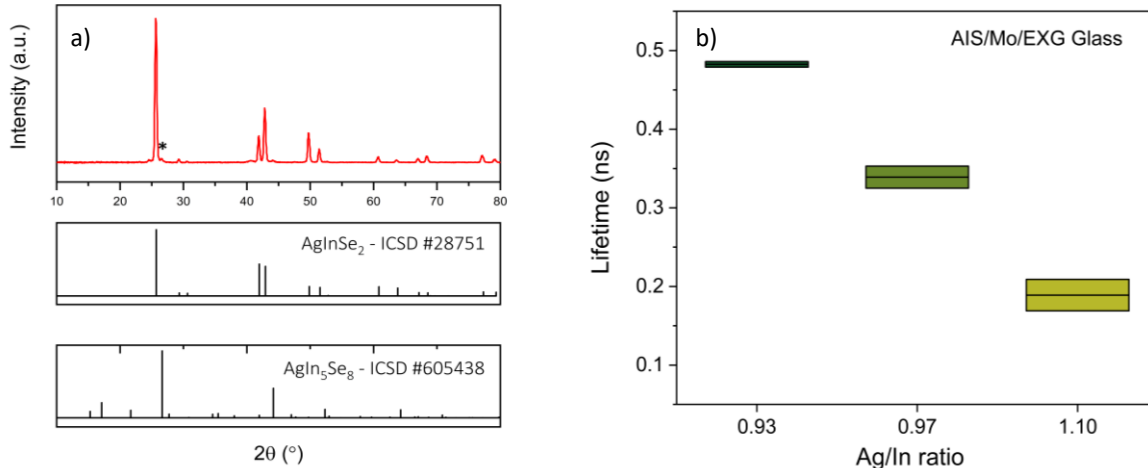


Figure 5. a) XRD pattern of AgInSe₂ film with Ag/In \sim 0.87 (* indicate AgIn₅Se₈ peak), b) Plot showing the variation of AgInSe₂ carrier lifetime with Ag/In ratio in the films selenized at 500 °C with regular selenization.

Annealing AgInSe₂ in Se rich atmosphere

The published literature on AgInSe₂/CuInSe₂/Cu(In,Ga)Se₂ has many instances of the detrimental effects of selenium vacancies on the absorber films. In a few cases, authors noted that growing AgInSe₂ in a Se-deficient environment could harm the material's crystallinity and electronic properties. Ema et al. observed that the phase pure chalcopyrite AgInSe₂ could only be produced when sufficient Se vapor was provided.³³ Patel et al. found that the AgInSe₂ films exhibited higher resistivity because of selenium deficiency.¹⁷ On similar grounds, Matsuo et al. pointed out that the AgInSe₂ samples annealed above 400 °C contained Ag and Se vacancies (V_{Ag} and V_{Se} , respectively).¹⁹ In CuInSe₂, selenium vacancies act as donors and provide electrons to the conduction band; similar phenomena may happen for AgInSe₂. In this regard, Abdel-Hady et al. noticed that the room temperature electron concentration varied between 10^{12} - 10^{18} cm⁻³ based on selenium deficiency for their n-type AgInSe₂ film.¹⁴ Thus, it is apparent that growing AgInSe₂ in a selenium-deficient environment could be deleterious.

The above discussion points towards that V_{Se} defects could potentially be harmful to the AgInSe₂ absorber films. Hence, we hypothesized that the photoluminescence yield and minority carrier lifetime in solution-processed AgInSe₂ would improve by increasing the selenium availability during selenization. Thus, our goal was to increase the selenium flux and maintain a selenium-rich environment during selenization to minimize defect formation while limiting the excess condensed selenium vapor on the final film.

We used various means to incorporate increased selenium in the films to test our hypothesis. Methods include using glass shims as the support for the substrate to increase selenium condensation on the film (**Figure 1b**), coating Se layers on top of as-coated AgInS₂, and dusting Se powder on AgInS₂ film before selenization. These methods are discussed in detail in the experimental section.

Improvements in Optoelectronic properties

The majority of literature noted AgInSe_2 to be an n-type material. Moreover, similar to CuInSe_2 , V_{Se} could be a deep donor defect in AgInSe_2 , which can act as recombination centers for minority carrier holes. If present in a high concentration, V_{Se} could harm the optoelectronic properties. Hence, we focused on incorporating increased selenium in the film during selenization.

Selenization on glass shims

During initial heat-up period, selenium is at a higher temperature than the AgInSe_2 film. Thus, selenizing the AgInSe_2 film on glass shims instead of directly on the graphite box floor would cause more selenium condensation on the film during the initial heat-up period and should help passivate the selenium-based defects. **Figures 6a and 6b** confirm the hypothesis as both the PL and lifetime improved with shims. Using this modified selenization setup, we achieved a minority carrier lifetime of around ~ 800 ps for an AgInSe_2 film with $\text{Ag/In} \sim 0.97$ compared to ~ 300 ps for the regular selenization with the same metal composition; the PL Yield (the area under the PL peak) also improved. We noted an increasing trend in lifetime and PL as the Ag/In ratio in the films decreased (**Figures 6c and 6d**), as observed previously for the films selenized without shims. The PL intensities and lifetime values were much higher with shims, and we observed a high lifetime of ~ 1.6 ns for $\text{Ag/In} \sim 0.91$. Since higher selenium availability is causing these improvements, other methods were also tested to increase the selenium availability during selenization. Raman mapping conducted on films selenized on shims only indicated the presence of AgInSe_2 based on 50 different Raman peaks, however, variations in relative peak intensity were present owing to discontinuities in the film (see **Figure S5**). We further note that in the temperature range of 475 °C to 515 °C, we did not observe any clear trend in the PL yield and lifetime with the selenization temperature when the samples were selenized on shims, **Figure S6**. This observation can be attributed to two opposing phenomena, grain growth, and selenium loss. We believe the grains would grow more significantly with higher selenization temperature which should contribute to reducing the number of grain boundary interfaces, possibly reducing the interaction of charge carriers with potential grain boundary defects and lowering the non-radiative recombination. This should, in turn, increase the PL yield and the carrier lifetime. However, a higher selenization temperature volatilizes and loses the available selenium faster due to its higher vapor pressure. This may cause some of the selenium from the film to volatilize, leading to selenium-based defects. These two competing effects possibly cause no trend in the lifetime with the selenization temperature.

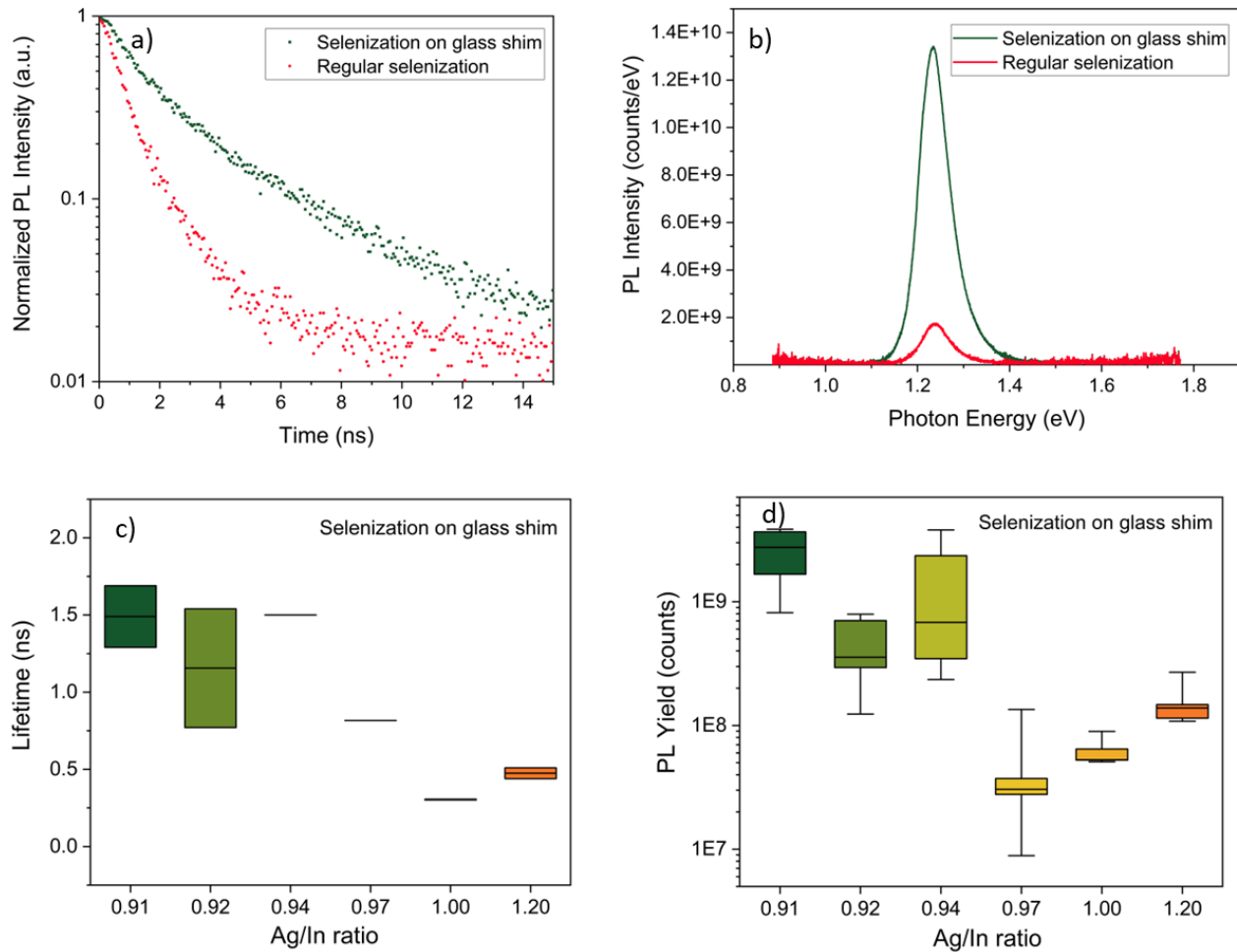


Figure 6. a) Difference in the TRPL decay curves, b) Difference in PL intensities for the AgInSe₂ film selenized on shims and the film selenized without shims at 500 °C with Ag/In ~ 0.92, c) Plot showing the variation in the carrier lifetime, and d) Plot showing the variation in the PL yield for the AgInSe₂ films with Ag/In ratio selenized at 500 °C using shims. The film stack is AgInSe₂/Mo/EXG Glass.

Incorporating increased selenium via different methods

As described in the experimental section, we tested two other methods to incorporate increased selenium, first by sprinkling ~ 50 mg selenium powder and another by coating two layers of selenium ink on the top of 0.5" x 1" as-coated sulfide film. We then selenized these films without shims using regular selenization at 600 °C. In both these cases, the photoluminescence yield was comparable to the film selenized on shims at the same conditions without any added selenium on top of the sulfide film (**Figure 7**). Moreover, the PL yield in both cases was much higher than the regular selenization without extra selenium incorporation. These results support our hypothesis that increased selenium supply benefits AgInSe₂ irrespective of the supply method used.

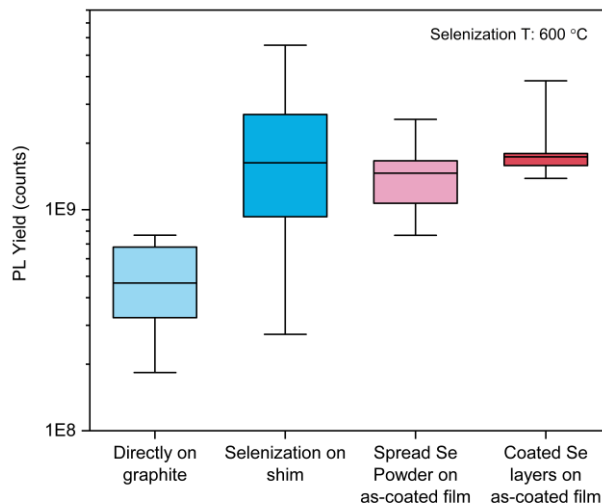


Figure 7. PL intensities for the different selenization approaches for AgInSe_2 films selenized at 600 °C.

Alumina as the back layer

In order to further increase the selenium condensation, DMF-TU-Chlorides ink was coated on an alumina-coated glass substrate instead of a molybdenum-coated glass substrate. The alumina has poorer heat transfer properties than the molybdenum, which slowed down the heat transfer to the film, driving higher selenium condensation. The alumina layer also has the propensity to prevent rapid nucleation and growth on its surface, resulting in top-down growth.³⁴ The results further confirm our hypothesis as the photoluminescence yield and lifetime improved significantly with the alumina at the back of the film, as shown in **Figures 8a and 8b**. **Figure 8c** compares the TRPL decay curves for the best films in the three cases, and the AgInSe_2 film on alumina-coated glass is superior. A high carrier lifetime of 9.22 ns was achieved for the film selenized using shims with alumina at the back. Theoretical V_{oc} calculations were also performed using the intensity-dependent Photoluminescence Quantum Yield (PLQY) calculations extrapolated to 1-sun. The film selenized on shims at 515 °C for 20 minutes achieved a high PLQY of 0.0128% (see **Figure S7**) and subsequently high theoretical V_{oc} of around 732 mV compared to 600 mV achieved by the film selenized directly on the graphite surface. It is worthwhile to note that we achieved these high numbers on the bare absorber film without any surface passivation. Without optimizing, we deposited a 50 nm layer of CdS on the absorber film, and the PLQY improved to 0.03%, achieving a theoretical V_{oc} of 754 mV. V_{oc} is a critical device parameter, and a V_{oc} above 700 mV is required for high-efficiency devices with a bandgap of around 1.2 eV. Also, this high PLQY suggests a maximum theoretical device efficiency of around 18%, inferred from the efficiency vs. PLQY% plot published elsewhere for different photovoltaic materials.³⁵ Hence, these results look promising for AgInSe_2 .

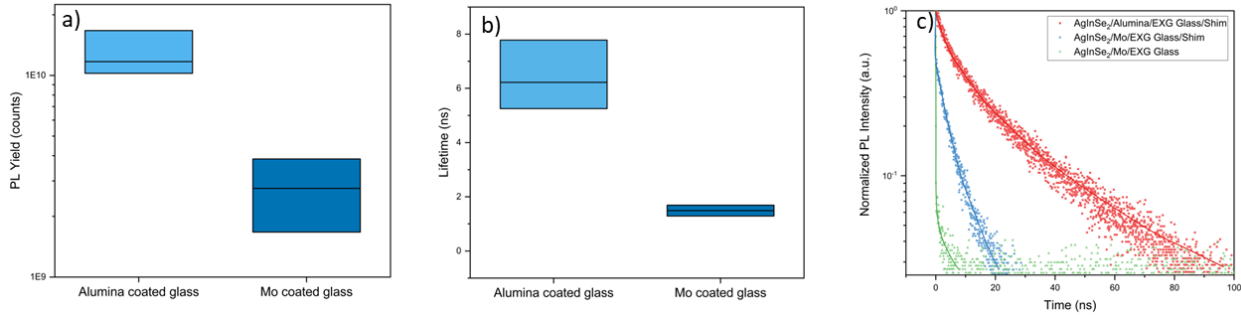


Figure 8. a) PL yield, b) Carrier lifetime for the AgInSe₂ films selenized with shims at 515 °C with Alumina and Molybdenum at the back respectively, and c) TRPL decay curves for the AgInSe₂ films selenized at 515 °C on shims with Alumina and Molybdenum at the back and the AgInSe₂ film selenized without shims and with Molybdenum back contact. These AgInSe₂ films have an Ag/In \sim 0.93.

XPS measurements confirm surface selenium amounts

We observed improvements in PL yield and lifetime whenever attempts were made to incorporate selenium in increased amounts. However, XRF, which has a precision of 0.5 at%, measured the same bulk selenium composition for all the samples. To verify the surface selenium content in the film, we conducted XPS analysis, which has a detection limit of approximately 0.1 at%. XPS data were collected from the Ag3d, In3d, and Se3d regions of both the film selenized on shims and film selenized directly on graphite. The XPS spectra are presented in **Figure S8**. The XPS analysis indicated a higher selenium content on the film's surface that was selenized on shims compared to the film selenized on graphite (**Table 1**). However, the bulk composition measured by the XRF remains nearly the same. This suggests a potential loss of selenium from the surface and near-surface regions, which may be affecting the optoelectronic properties.

Table 1. Comparison of the surface and bulk compositions of AgInSe₂ films selenized on graphite and selenized on shim analyzed by XPS and XRF, respectively.

	AgInSe ₂ selenized on graphite	AgInSe ₂ selenized on shim
Surface Composition (XPS)	Ag _{0.64} In ₁ Se _{1.2}	Ag _{0.52} In ₁ Se _{1.5}
Bulk Composition (XRF)	Ag _{0.94} In ₁ Se _{2.3}	Ag _{0.92} In ₁ Se _{2.3}

Continuous film formation

Till now, we have achieved excellent optoelectronic properties for AgInSe₂ films, but the films are rather non-homogenous, as shown in **Figures S9, S10, S11, and S12**. They have large disconnected grains, possibly because of the excessive growth in the out-of-plane direction. Hence, there was a need to achieve a thicker film so that grains grow enough laterally and a continuous film is achieved. We achieved a relatively continuous film using shims after

selenization when started with 1.2 M total metal concentration, coated 10 layers and selenized at 600 °C, as shown in **Figures 9a and 9b**. However, we only achieved an estimated V_{oc} of 700 mV for this film through PLQY analysis, which was slightly lower than the films selenized at lower temperatures. This is partially due to the inability to maintain a saturated selenium environment at 600 °C for 20 min due to the high vapor pressure of selenium and, therefore, increased selenium leakage rate from the box during annealing and cool down. We again connect this to the selenium-based defects. The grain size improved upon selenization at higher temperatures, which should have reduced the grain boundary recombination, but some other defects seem to affect the performance of higher-temperature films. We hypothesize that increased selenium loss from the film at higher temperatures could limit the performance. In other words, selenium vacancies were possibly formed in AgInSe_2 film by selenizing at higher temperatures in an insufficient selenium environment and during cooldown. Nonetheless, we again passivated this film with a 50 nm thick layer of CdS, and it improved the V_{oc} to 741 mV with a PLQY of 0.019%.

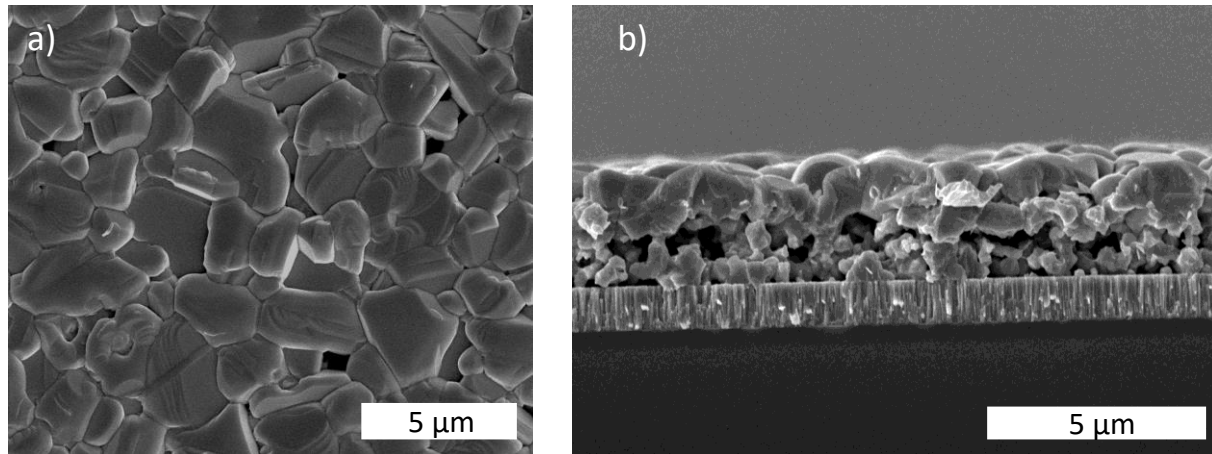


Figure 9. a) SEM top-view, and b) SEM cross-sectional view of AgInSe_2 film prepared from 1.2 M conc. ink with $\text{Ag/In} \sim 0.93$ and selenized at 600 °C.

We further performed Hall effect measurements on a similar film to obtain the carrier properties. We swept the magnetic field from -9 to 4 T and recorded the room temperature Hall voltage, shown in **Figure S13**. On data analysis, we obtained an n-type conductivity for the AgInSe_2 film with a low carrier mobility of $1.2 \text{ cm}^2/\text{V.s}$, possibly because of the thick fine grain layer at the bottom of the film and a moderate carrier concentration of 10^{14} cm^{-3} . The XPS measurements near the valence band maximum further confirmed the n-type conductivity. The analysis suggests an energy gap of 0.68 eV between the Fermi-level (E_F) and the valence edge position (E_V), whereas the bandgap is 1.25 eV. Both p-n and p-i-n heterojunctions may be possible for these moderate carrier concentrations. However, the choice of hole and electron transport layers is not immediately obvious.

We further tried to match various materials with the band positions reported for AgInSe_2 for the electron and hole transport layers.³⁶ CdS has a significant conduction band offset (~ 0.35 eV) with AgInSe_2 , whereas NiTiO_3 has a conduction band offset of ~ 0.15 eV.^{37,38} On the other hand, MnS has a suitable valence edge location with high hole concentration and could be a viable option for the hole transport layer.³⁶ Future work will explore the p-i-n architecture for AgInSe_2 using

the materials mentioned earlier and other novel hole and electron transport layers to fabricate a solar device.

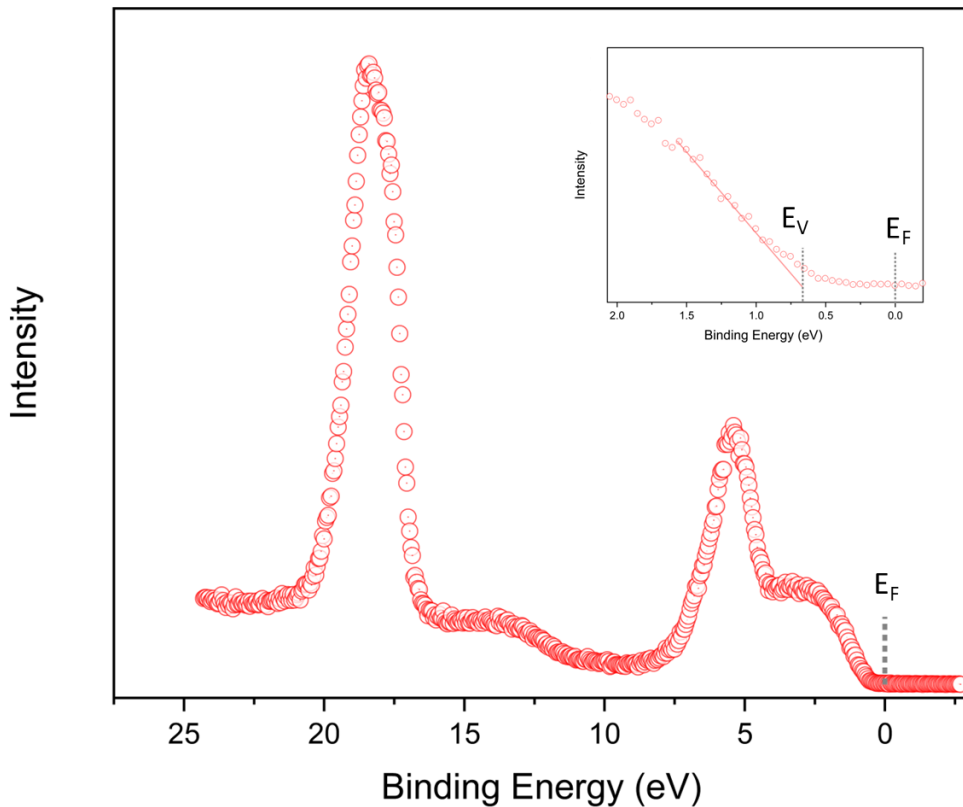


Figure 10. Valence band spectra for AgInSe_2 film prepared from 1.2 M conc. ink with $\text{Ag}/\text{In} \sim 0.93$ and selenized at 600°C . The position of the valence band edge with respect to the Fermi level is marked.

Conclusions

AgInSe_2 is a promising photo absorber with a high absorption coefficient, suitable bandgap, and n-type conductivity. We implemented the DMF-TU-Chlorides chemistry to synthesize a high-quality solution-processed AgInSe_2 thin film. Our study shows that selenium-based defects harm AgInSe_2 and seriously affect optoelectronic properties. A careful study was performed to incorporate increased selenium during the heat treatment and improve the optoelectronic properties. We achieved a lifetime of 9.2 ns, PLQY of 0.013%, and a theoretical estimated V_{oc} of 732 mV without surface passivation.

Further improvements in the photoluminescence were observed after passivation with CdS . These exciting optoelectronic properties motivate to synthesize an AgInSe_2 -based solar cell but moderate carrier concentration of 10^{14} cm^{-3} measured from the Hall effect measurements suggest that the p-n heterojunction may not be suitable for this low carrier concentration, requiring consideration of alternate architectures such as p-i-n solar cells.

Conflicts of interest

There are no conflicts to declare.

Acknowledgments

The authors are grateful for the financial support from the National Science Foundation through Grants 1735282-NRT (SFEWS) and 10001536 (INFEWS). The authors would like to thank Jonathan Turnley, Apurva Pradhan, and Dr. Dmitry Zemlyanov for their valuable suggestions related to the project. The XPS data were obtained at the Surface Analysis Facility of the Birck Nanotechnology Center at Purdue University.

References

- (1) Green, M. A.; Hishikawa, Y.; Dunlop, E. D.; Levi, D. H.; Hohl-Ebinger, J.; Yoshita, M.; Ho-Baillie, A. W. Y. Solar Cell Efficiency Tables (Version 53). *Progress in Photovoltaics: Research and Applications* 2019, 27 (1), 3–12. <https://doi.org/10.1002/pip.3102>.
- (2) Ahmadpanah, F. S.; Orouji, A. A.; Gharibshahian, I. Improving the Efficiency of CIGS Solar Cells Using an Optimized P-Type CZTSSe Electron Reflector Layer. *Journal of Materials Science: Materials in Electronics* 2021, 32 (17), 22535–22547. <https://doi.org/10.1007/s10854-021-06740-6>.
- (3) Todorov, T. K.; Gunawan, O.; Gokmen, T.; Mitzi, D. B. Solution-Processed Cu(In,Ga)(S,Se)2 Absorber Yielding a 15.2% Efficient Solar Cell. *Progress in Photovoltaics: Research and Applications* 2013, 21 (1), 82–87. <https://doi.org/10.1002/pip.1253>.
- (4) Romanyuk, Y. E.; Hagendorfer, H.; Stücheli, P.; Fuchs, P.; Uhl, A. R.; Sutter-Fella, C. M.; Werner, M.; Haass, S.; Stückelberger, J.; Broussillou, C.; Grand, P. P.; Bermudez, V.; Tiwari, A. N. All Solution-Processed Chalcogenide Solar Cells - From Single Functional Layers Towards a 13.8% Efficient CIGS Device. *Adv Funct Mater* 2015, 25 (1), 12–27. <https://doi.org/10.1002/adfm.201402288>.
- (5) Awasthi, V.; Pandey, S. K.; Pandey, S. K.; Verma, S.; Gupta, M.; Mukherjee, S. Growth and Characterizations of Dual Ion Beam Sputtered CIGS Thin Films for Photovoltaic Applications. *Journal of Materials Science: Materials in Electronics* 2014, 25 (7), 3069–3076. <https://doi.org/10.1007/s10854-014-1985-0>.

(6) Suresh, S.; Uhl, A. R. Present Status of Solution-Processing Routes for Cu(In,Ga)(S,Se)2 Solar Cell Absorbers. *Advanced Energy Materials*. John Wiley and Sons Inc. April 1, 2021. <https://doi.org/10.1002/aenm.202003743>.

(7) Clark, J. A.; Murray, A.; Lee, J. M.; Autrey, T. S.; Collord, A. D.; Hillhouse, H. W. Complexation Chemistry in N, N-Dimethylformamide-Based Molecular Inks for Chalcogenide Semiconductors and Photovoltaic Devices. *J Am Chem Soc* 2019, 141 (1), 298–308. <https://doi.org/10.1021/jacs.8b09966>.

(8) Shannon, R. D. Revised Effective Ionic Radii and Systematic Studies of Interatomic Distances in Halides and Chalcogenides. *Acta Crystallographica Section A* 1976, 32 (5), 751–767. <https://doi.org/10.1107/S0567739476001551>.

(9) Maeda, T.; Takeichi, T.; Wada, T. Systematic Studies on Electronic Structures of CuInSe 2 and the Other Chalcopyrite Related Compounds by First Principles Calculations. *Physica Status Solidi (A) Applications and Materials Science* 2006, 203 (11), 2634–2638. <https://doi.org/10.1002/pssa.200669539>.

(10) Tell, B.; Shay, J. L.; Kasper, H. M. Room-Temperature Electrical Properties of Ten I-III-VI2 Semiconductors. *J Appl Phys* 1972, 43 (5), 2469–2470. <https://doi.org/10.1063/1.1661532>.

(11) Mustafa, H.; Hunter, D.; Pradhan, A. K.; Roy, U. N.; Cui, Y.; Burger, A. Synthesis and Characterization of AgInSe2 for Application in Thin Film Solar Cells. *Thin Solid Films* 2007, 515 (17), 7001–7004. <https://doi.org/10.1016/j.tsf.2007.02.054>.

(12) Valdes, N.; Lee, J. W.; Shafarman, W. Comparison of Ag and Ga Alloying in Low Bandgap CuInSe2 -Based Solar Cells. *Solar Energy Materials and Solar Cells* 2019, 195, 155–159. <https://doi.org/10.1016/j.solmat.2019.02.022>.

(13) Sopiha, K. V.; Larsen, J. K.; Donzel-Gargand, O.; Khavari, F.; Keller, J.; Edoff, M.; Platzer-Björkman, C.; Persson, C.; Scragg, J. J. S. Thermodynamic Stability, Phase Separation and Ag Grading in (Ag,Cu)(In,Ga)Se2solar Absorbers. *J Mater Chem A Mater* 2020, 8 (17), 8740–8751. <https://doi.org/10.1039/d0ta00363h>.

(14) Abdel-Hady, D.; Salem, A. M. Electrical Resistivity of AgInSe₂ Films; Elsevier, 1997; Vol. 242. [https://doi.org/10.1016/S0378-4371\(97\)00200-8](https://doi.org/10.1016/S0378-4371(97)00200-8).

(15) Arredondo, C. A.; Gordillo, G. Photoconductive and Electrical Transport Properties of AgInSe₂ Thin Films Prepared by Co-Evaporation. *Physica B Condens Matter* 2010, 405 (17), 3694–3699. <https://doi.org/10.1016/j.physb.2010.05.068>.

(16) Al-Agel, F. A.; Mahmoud, W. E. Synthesis and Characterization of AIS Chalcopyrite Thin Films for Solar Cell Applications. *Mater Lett* 2012, 82, 82–84. <https://doi.org/10.1016/j.matlet.2012.05.065>.

(17) Patel, S. M.; Patel, A. D. Electrical resistivity of polycrystalline AgInSe₂ thin films. *Materials Letters* 1983, Vol 2, Issue 2, 127-130. [https://doi.org/10.1016/0167-577X\(83\)90052-6](https://doi.org/10.1016/0167-577X(83)90052-6).

(18) Ramesh, P. P.; Naidu, P. J.; Reddy, A. M. A. Optical Absorption Studies on Single-Phase Polycrystalline AgInSe₂ Thin Films; 1996, 15, 116–119. <https://doi.org/10.1007/BF00291442>.

(19) Matsuo, H.; Yoshino, K.; Ikari, T. Preparation of AgInSe₂ Thin Films Grown by Vacuum Evaporation Method. In *Physica Status Solidi (C) Current Topics in Solid State Physics*; 2006; Vol. 3, pp 2644–2647. <https://doi.org/10.1002/pssc.200669511>.

(20) Kaleli, M.; Çolakoğlu, T.; Parlak, M. Production and Characterization of Layer by Layer Sputtered Single-Phase AgInSe₂ Thin Film by Thermal Selenization. *Appl Surf Sci* 2013, 286, 171–176. <https://doi.org/10.1016/j.apsusc.2013.09.043>.

(21) Santhosh Kumar, M. C.; Pradeep, B. Formation and Properties of AgInSe₂ Thin Films by Co-Evaporation. *Vacuum* 2004, 72 (4), 369–378. <https://doi.org/10.1016/j.vacuum.2003.09.008>.

(22) Scheer, R.; Schock, H. Chalcogenide Photovoltaics; Wiley, 2011. <https://doi.org/10.1002/9783527633708>.

(23) Nakamura, M.; Yamaguchi, K.; Kimoto, Y.; Yasaki, Y.; Kato, T.; Sugimoto, H. Cd-Free Cu(In,Ga)(Se,S)₂ Thin-Film Solar Cell with Record Efficiency of 23.35%. *IEEE J Photovolt* 2019, 9 (6), 1863–1867. <https://doi.org/10.1109/JPHOTOV.2019.2937218>.

(24) Walker, B. C.; Agrawal, R. Contamination-Free Solutions of Selenium in Amines for Nanoparticle Synthesis. *Chemical Communications* 2014, 50 (61), 8331–8334. <https://doi.org/10.1039/c4cc02379j>.

(25) Rokke, D. Deposition and Characterization of Solution-Processed Chalcogenides for Photovoltaic Applications. *Purdue University*, 2022.

(26) Guo, Q.; Ford, G. M.; Hillhouse, H. W.; Agrawal, R. Sulfide Nanocrystal Inks for Dense $\text{Cu}(\text{In}_{1-x}\text{Ga}_x)(\text{S}_{1-y}\text{Se}_y)_2$ Absorber Films and Their Photovoltaic Performance. *Nano Lett* 2009, 9 (8), 3060–3065. <https://doi.org/10.1021/nl901538w>.

(27) Kyle Weidemann. Development and Characterization of Film Formation Processes Toward the Improved Performance of Solution-Processed Semiconducting Thin Films. *Purdue University* 2022.

(28) Pradhan, A. A.; Uible, M. C.; Agarwal, S.; Turnley, J. W.; Khandelwal, S.; Peterson, J. M.; Blach, D. D.; Swope, R. N.; Huang, L.; Bart, S. C.; Agrawal, R. Synthesis of BaZrS_3 and BaHfS_3 Chalcogenide Perovskite Films Using Single-Phase Molecular Precursors at Moderate Temperatures. *Angewandte Chemie International Edition* 2023, 62 (15). <https://doi.org/10.1002/anie.202301049>.

(29) McLeod, S.; Alruqobah, E.; Agrawal, R. Liquid Assisted Grain Growth in Solution Processed $\text{Cu}(\text{In},\text{Ga})(\text{S},\text{Se})_2$. *Solar Energy Materials and Solar Cells* 2019, 195, 12–23. <https://doi.org/10.1016/j.solmat.2019.02.020>.

(30) Hages, C. J.; Koeper, M. J.; Miskin, C. K.; Brew, K. W.; Agrawal, R. Controlled Grain Growth for High-Performance Nanoparticle-Based Kesterite Solar Cells. *Chemistry of Materials* 2016, 28 (21), 7703–7714. <https://doi.org/10.1021/acs.chemmater.6b02733>.

(31) Vincent, K. C.; Agarwal, S.; Turnley, J. W.; Agrawal, R. Liquid Flux–Assisted Mechanism for Modest Temperature Synthesis of Large-Grain BaZrS_3 and BaHfS_3 Chalcogenide Perovskites. *Advanced Energy and Sustainability Research* 2023, 4 (5). <https://doi.org/10.1002/aesr.202300010>.

(32) Zhang, S. B.; Wei, S.-H.; Zunger, A.; Katayama-Yoshida, H. Defect Physics of the CuInSe₂ Chalcopyrite Semiconductor. *Phys Rev B* 1998, 57 (16), 9642–9656. <https://doi.org/10.1103/PhysRevB.57.9642>.

(33) Ema, Y.; Harakawa, N. Formation and Properties of AgInSe₂ Thin Films Deposited from Alloy Chunks. *Jpn. J. Appl. Phys.* 1995, 34 3260. DOI 10.1143/JJAP.34.3260.

(34) Deshmukh, S. D.; Weideman, K. G.; Ellis, R. G.; Kisslinger, K.; Agrawal, R. Enabling Fine-Grain Free 2-Micron Thick CISe/CIGSe Film Fabrication via a Non-Hydrazine Based Solution Processing Route. *Mater Adv* 2022, 3 (7), 3293–3302. <https://doi.org/10.1039/D2MA00095D>.

(35) Green, M. A.; Ho-Baillie, A. W. Y. Pushing to the Limit: Radiative Efficiencies of Recent Mainstream and Emerging Solar Cells. *ACS Energy Lett* 2019, 4 (7), 1639–1644. <https://doi.org/10.1021/acsenergylett.9b01128>.

(36) Keller, J.; Sopiha, K. V.; Stolt, O.; Stolt, L.; Persson, C.; Scragg, J. J. S.; Törndahl, T.; Edoff, M. Wide-gap (Ag,Cu)(In,Ga)Se 2 Solar Cells with Different Buffer Materials—A Path to a Better Heterojunction. *Progress in Photovoltaics: Research and Applications* 2020, 28 (4), 237–250. <https://doi.org/10.1002/pip.3232>.

(37) Stoffel, N. G. Experimental Band Structure of Cadmium Sulfide. *Phys Rev B* 1983, 28 (6), 3306–3319. <https://doi.org/10.1103/PhysRevB.28.3306>.

(38) Inceesungvorn, B.; Teeranunpong, T.; Nunkaew, J.; Suntalelat, S.; Tantraviwat, D. Novel NiTiO₃/Ag₃VO₄ Composite with Enhanced Photocatalytic Performance under Visible Light. *Catal Commun* 2014, 54, 35–38. <https://doi.org/10.1016/j.catcom.2014.05.015>.